Optimum Aerodynamic Design using the Navier–Stokes Equations

A. Jameson [*], N.A. Pierce [†] and L. Martinelli [§]

[*, §] *Department of Mechanical and Aerospace Engineering*
Princeton University
Princeton, New Jersey 08544 USA

and

[†] *Oxford University Computing Laboratory*
Numerical Analysis Group
Oxford OX1 3QD UK

ABSTRACT

This paper describes the formulation of optimization techniques based on control theory for aerodynamic shape design in viscous compressible flow, modelled by the Navier-Stokes equations. It extends previous work on optimization for inviscid flow. The theory is applied to a system defined by the partial differential equations of the flow, with the boundary shape acting as the control. The Frechet derivative of the cost function is determined via the solution of an adjoint partial differential equation, and the boundary shape is then modified in a direction of descent. This process is repeated until an optimum solution is approached. Each design cycle requires the numerical solution of both the flow and the adjoint equations, leading to a computational cost roughly equal to the cost of two flow solutions. The cost is kept low by using multigrid techniques, in conjunction with preconditioning to accelerate the convergence of the solutions. The power of the method is illustrated by designs of wings and wing-body combinations for long range transport aircraft. Satisfactory designs are usually obtained with 20-40 design cycles.

1 INTRODUCTION

This paper, which is dedicated to Sir James Lighthill, is focused on the problem of aerodynamic design. Here, as in so many other branches of fluid mechanics and applied mathematics, Lighthill has made a seminal contribution through his early demonstration of a solution of the inverse problem for airfoil design in potential flow [1].

The evolution of computational fluid dynamics during the last three decades has made possible the rapid evaluation of alternative designs by computational simulation, eliminating the need to build numerous models for wind tunnel testing, which is used primarily to confirm the performance of the final design, and to provide a complete database for the full flight envelope. The designer still needs some guiding principle to distinguish a good design out of an infinite number of possible variations, since it is not at all likely that a truly optimum design can be found by a trial and error process. This motivates the use of numerical optimization procedures in conjunction with computational flow simulations.

Early investigations into aerodynamic optimization relied on direct evaluation of the influence of each design variable. This dependence was estimated by separately varying each design parameter and recalculating the flow. The computational cost of this method is proportional to the number of design variables and consequently becomes prohibitive as the number of design parameters is increased.

An alternative approach to design relies on the fact that experienced designers generally have an intuitive feel for the kind of pressure distribution that will provide the desired aerodynamic performance. This motivates the introduction of inverse problems in which the shape corresponding to a specified pressure distribution is to be determined. A complete analysis of the inverse problem

for airfoils in two dimensional potential flow was given by Lighthill [1], who obtained a solution by conformally mapping the profile to a unit circle. The speed over the profile is

$$q = \frac{1}{h} |\nabla \phi|$$

where ϕ is the potential, which is known for the circle, while h is the modulus of the mapping function. The surface value of h can be obtained by setting $q = q_d$, where q_d is the desired speed, and since the mapping function is analytic, it is uniquely determined by the value of h on the boundary. Lighthill's analysis highlights the fact that a physically realizable shape may not exist unless the prescribed pressure distribution satisfies certain constraints. In fact a solution exists for a given speed q_∞ at infinity only if

$$\frac{1}{2\pi} \oint q_d d\theta = q_\infty$$

where θ is the polar angle around the circle, and there are additional constraints on q_d if the profile is to be closed.

In the more general case of three-dimensional viscous compressible flow, the constraints which must be satisfied by a realizable target pressure distribution are not known, and attempts to enforce an unrealizable pressure distribution as a boundary condition can lead to an ill-posed problem. The problems of optimal and inverse design can both be systematically treated within the mathematical theory for the control of systems governed by partial differential equations [2] by regarding the design problem as a control problem in which the control is the shape of the boundary. The inverse problem then becomes a special case of the optimal design problem in which the shape changes are driven by the discrepancy between the current and target pressure distributions.

The control theory approach to optimal aerodynamic design, in which shape changes are based on gradient information obtained by solution of an adjoint problem, was first applied to transonic flow by Jameson [3,4]. He formulated the method for inviscid compressible flows with shocks governed by both the potential equation and the Euler equations [3,5,6]. With this approach, the cost of a design cycle is independent of the number of design variables. When applied to the design of the airfoils in compressible potential flow using conformal mapping to transform the computational domain to a unit disk, it leads to a natural generalization of Lighthill's method. The effects of compressibility are represented by an additional term in the modification of the mapping function which tends to zero as the Mach number tends to zero [3,5]. More recently, the method has been employed for wing design in the context of complex aircraft configurations [7,8], using a grid perturbation technique to accommodate the geometry modifications.

Pironneau had earlier initiated studies of the use of control theory for optimum shape design of systems governed by elliptic equations [9,10]. Ta'asan, Kuruvila and Salas have proposed a one shot approach in which the constraint represented by the flow equations need only be satisfied by the final converged design solution [11]. Adjoint methods have also been used by Baysal and Eleshaky [12], by Cabuk and Modi [13,14], and by Desai and Ito [15].

The objective of the present work is the extension of adjoint methods for optimal aerodynamic design to flows governed by the compressible Navier–Stokes equations. While inviscid formulations have proven useful for the design of transonic wings at cruise conditions, the inclusion of boundary layer displacement effects with viscous design provides increased realism and alleviates shocks that would otherwise form in the viscous solution over the final inviscid design. Accurate resolution of viscous effects such as separation and shock/boundary layer interaction is also essential for optimal design encompassing off-design conditions and high-lift configurations.

The computational costs of viscous design are at least an order of magnitude greater than for design using the Euler equations for several reasons. First, the number of mesh points must be increased by a factor of two or more to resolve the boundary layer. Second, there is the additional cost of computing the viscous terms and a turbulence model. Finally, Navier–Stokes calculations generally converge much more slowly than Euler solutions due to discrete stiffness and directional decoupling arising from the highly stretched boundary layer cells. The computational feasibility of viscous design therefore hinges on the development of a rapidly convergent Navier–Stokes flow solver. Pierce and Giles have developed a preconditioned multigrid method that dramatically improves

convergence of viscous calculations by ensuring that all error modes inside the stretched boundary layer cells are damped efficiently [16,17]. The same acceleration techniques are applicable to the adjoint calculation, so that the potential payoffs toward reducing the cost of the design process are substantial.

The ultimate success of an aircraft design depends on the resolution of complex multi-disciplinary trade-offs between factors such as aerodynamic efficiency, structural weight, stability and control, and the volume required to contain fuel and payload. A design is finalized only after numerous iterations, cycling between the disciplines. The development of accurate and efficient methods for aerodynamic shape optimization represents a worthwhile intermediate step towards the eventual goal of full multi-disciplinary optimal design.

2 GENERAL FORMULATION OF THE ADJOINT APPROACH TO OPTIMAL DESIGN

Before embarking on a detailed derivation of the adjoint formulation for optimal design using the Navier–Stokes equations, it is helpful to summarize the general abstract description of the adjoint approach which has been thoroughly documented in references [3,4].

The progress of the design procedure is measured in terms of a cost function I, which could be, for example the drag coefficient or the lift to drag ratio. For flow about an airfoil or wing, the aerodynamic properties which define the cost function are functions of the flow-field variables (w) and the physical location of the boundary, which may be represented by the function $\mathcal{F}$, say. Then

$$I = I\left(w, \mathcal{F}\right),$$

and a change in $\mathcal{F}$ results in a change

$$\delta I = \left[\frac{\partial I^T}{\partial w}\right]_I \delta w + \left[\frac{\partial I^T}{\partial \mathcal{F}}\right]_{II} \delta \mathcal{F}, \tag{1}$$

in the cost function. Here, the subscripts I and II are used to distinguish the contributions due to the variation δw in the flow solution from the change associated directly with the modification $\delta\mathcal{F}$ in the shape. This notation is introduced to assist in grouping the numerous terms that arise during the derivation of the full Navier–Stokes adjoint operator, so that it remains feasible to recognize the basic structure of the approach as it is sketched in the present section.

Using control theory, the governing equations of the flow field are introduced as a constraint in such a way that the final expression for the gradient does not require multiple flow solutions. This corresponds to eliminating δw from (1).

Suppose that the governing equation R which expresses the dependence of w and $\mathcal{F}$ within the flow-field domain $\mathcal{D}$ can be written as

$$R\left(w, \mathcal{F}\right) = 0. \tag{2}$$

Then δw is determined from the equation

$$\delta R = \left[\frac{\partial R}{\partial w}\right]_I \delta w + \left[\frac{\partial R}{\partial \mathcal{F}}\right]_{II} \delta \mathcal{F} = 0. \tag{3}$$

Next, introducing a Lagrange Multiplier ψ, we have

$$\begin{aligned} \delta I &= \frac{\partial I^T}{\partial w}\delta w + \frac{\partial I^T}{\partial \mathcal{F}}\delta\mathcal{F} - \psi^T\left(\left[\frac{\partial R}{\partial w}\right]\delta w + \left[\frac{\partial R}{\partial \mathcal{F}}\right]\delta\mathcal{F}\right) \\ &= \left\{\frac{\partial I^T}{\partial w} - \psi^T\left[\frac{\partial R}{\partial w}\right]\right\}_I \delta w + \left\{\frac{\partial I^T}{\partial \mathcal{F}} - \psi^T\left[\frac{\partial R}{\partial \mathcal{F}}\right]\right\}_{II} \delta\mathcal{F}. \end{aligned} \tag{4}$$

Choosing ψ to satisfy the adjoint equation

$$\left[\frac{\partial R}{\partial w}\right]^T \psi = \frac{\partial I}{\partial w} \tag{5}$$

the first term is eliminated, and we find that

$$\delta I = \mathcal{G}\delta\mathcal{F}, \tag{6}$$

where

$$\mathcal{G} = \frac{\partial I^T}{\partial \mathcal{F}} - \psi^T \left[\frac{\partial R}{\partial \mathcal{F}}\right].$$

The advantage is that (6) is independent of δw, with the result that the gradient of I with respect to an arbitrary number of design variables can be determined without the need for additional flow-field evaluations. In the case that (2) is a partial differential equation, the adjoint equation (5) is also a partial differential equation and determination of the appropriate boundary conditions requires careful mathematical treatment.

The computational cost of a single design cycle is roughly equivalent to the cost of two flow solutions since the the adjoint problem has similar complexity. When the number of design variables becomes large, the computational efficiency of the control theory approach over traditional approach, which requires direct evaluation of the gradients by individually varying each design variable and recomputing the flow field, becomes compelling.

Once equation (3) is established, an improvement can be made with a shape change

$$\delta\mathcal{F} = -\lambda\mathcal{G}$$

where λ is positive, and small enough that the first variation is an accurate estimate of δI. The variation in the cost function then becomes

$$\delta I = -\lambda\mathcal{G}^T\mathcal{G} < 0.$$

After making such a modification, the gradient can be recalculated and the process repeated to follow a path of steepest descent until a minimum is reached. In order to avoid violating constraints, such as a minimum acceptable wing thickness, the gradient may be projected into an allowable subspace within which the constraints are satisfied. In this way, procedures can be devised which must necessarily converge at least to a local minimum.

3 THE NAVIER-STOKES EQUATIONS

For the derivations that follow, it is convenient to use Cartesian coordinates (x_1,x_2,x_3) and to adopt the convention of indicial notation where a repeated index "i" implies summation over $i = 1$ to 3. The three-dimensional Navier-Stokes equations then take the form

$$\frac{\partial w}{\partial t} + \frac{\partial f_i}{\partial x_i} = \frac{\partial f_{vi}}{\partial x_i} \quad \text{in } \mathcal{D}, \tag{7}$$

where the state vector w, inviscid flux vector f and viscous flux vector f_v are described respectively by

$$w = \left\{ \begin{array}{c} \rho \\ \rho u_1 \\ \rho u_2 \\ \rho u_3 \\ \rho E \end{array} \right\}, \tag{8}$$

$$f_i = \left\{ \begin{array}{c} \rho u_i \\ \rho u_i u_1 + p\delta_{i1} \\ \rho u_i u_2 + p\delta_{i2} \\ \rho u_i u_3 + p\delta_{i3} \\ \rho u_i H \end{array} \right\}, \tag{9}$$

$$f_{vi} = \left\{ \begin{array}{c} 0 \\ \sigma_{ij}\delta_{j1} \\ \sigma_{ij}\delta_{j2} \\ \sigma_{ij}\delta_{j3} \\ u_j\sigma_{ij} + k\frac{\partial T}{\partial x_i} \end{array} \right\}. \tag{10}$$

In these definitions, ρ is the density, u_1, u_2, u_3 are the Cartesian velocity components, E is the total energy and δ_{ij} is the Kronecker delta function. The pressure is determined by the equation of state

$$p = (\gamma - 1)\,\rho\left\{E - \frac{1}{2}\,(u_i u_i)\right\},$$

and the stagnation enthalpy is given by

$$H = E + \frac{p}{\rho},$$

where γ is the ratio of the specific heats. The viscous stresses may be written as

$$\sigma_{ij} = \mu\left(\frac{\partial u_i}{\partial x_j} + \frac{\partial u_j}{\partial x_i}\right) + \lambda\delta_{ij}\frac{\partial u_k}{\partial x_k}, \tag{11}$$

where μ and λ are the first and second coefficients of viscosity. The coefficient of thermal conductivity and the temperature are computed as

$$k = \frac{c_p\mu}{Pr}, \qquad T = \frac{p}{R\rho}, \tag{12}$$

where Pr is the Prandtl number, c_p is the specific heat at constant pressure, and R is the gas constant.

For discussion of real applications using a discretization on a body conforming structured mesh, it is also useful to consider a transformation to the computational coordinates (ξ_1,ξ_2,ξ_3) defined by the metrics

$$K_{ij} = \left[\frac{\partial x_i}{\partial \xi_j}\right], \quad J = \det(K), \quad K_{ij}^{-1} = \left[\frac{\partial \xi_i}{\partial x_j}\right].$$

The Navier-Stokes equations can then be written in computational space as

$$\frac{\partial\,(Jw)}{\partial t} + \frac{\partial\,(F_i - F_{vi})}{\partial \xi_i} = 0 \quad \text{in } \mathcal{D}, \tag{13}$$

where the inviscid and viscous flux contributions are now defined with respect to the computational cell faces by $F_i = S_{ij}f_j$ and $F_{vi} = S_{ij}f_{vj}$, and the quantity $S_{ij} = JK_{ij}^{-1}$ is used to represent the projection of the ξ_i cell face along the x_j axis. In obtaining equation (13) we have made use of the property that

$$\frac{\partial S_{ij}}{\partial \xi_i} = 0 \tag{14}$$

which represents the fact that the sum of the face areas over a closed volume is zero, as can be readily verified by a direct examination of the metric terms.

4 GENERAL FORMULATION OF THE OPTIMAL DESIGN PROBLEM FOR THE NAVIER-STOKES EQUATIONS

Aerodynamic optimization is based on the determination of the effect of shape modifications on some performance measure which depends on the flow. For convenience, the coordinates ξ_i describing the fixed computational domain are chosen so that each boundary conforms to a constant value of one of these coordinates. Variations in the shape then result in corresponding variations in the mapping derivatives defined by K_{ij}.

Suppose that the performance is measured by a cost function

$$I = \int_{\mathcal{B}} \mathcal{M}\left(w, S\right) d\mathcal{B}_\xi + \int_{\mathcal{D}} \mathcal{P}\left(w, S\right) d\mathcal{D}_\xi,$$

containing both boundary and field contributions where $d\mathcal{B}_\xi$ and $d\mathcal{D}_\xi$ are the surface and volume elements in the computational domain. In general, $\mathcal{M}$ and $\mathcal{P}$ will depend on both the flow variables w and the metrics S defining the computational space.

The design problem is now treated as a control problem where the boundary shape represents the control function, which is chosen to minimize I subject to the constraints defined by the flow equations (13). A shape change produces a variation in the flow solution δw and the metrics δS which in turn produce a variation in the cost function

$$\delta I = \int_{\mathcal{B}} \delta\mathcal{M}(w, S) \, d\mathcal{B}_\xi + \int_{\mathcal{D}} \delta\mathcal{P}(w, S) \, d\mathcal{D}_\xi, \tag{15}$$

with

$$\begin{aligned} \delta\mathcal{M} &= \left[\mathcal{M}_w\right]_I \delta w + \delta\mathcal{M}_{II}, \\ \delta\mathcal{P} &= \left[\mathcal{P}_w\right]_I \delta w + \delta\mathcal{P}_{II}, \end{aligned} \tag{16}$$

where we continue to use the subscripts I and II to distinguish between the contributions associated with the variation of the flow solution δw and those associated with the metric variations δS. Thus $\left[\mathcal{M}_w\right]_I$ and $\left[\mathcal{P}_w\right]_I$ represent $\frac{\partial\mathcal{M}}{\partial w}$ and $\frac{\partial\mathcal{P}}{\partial w}$ with the metrics fixed, while $\delta\mathcal{M}_{II}$ and $\delta\mathcal{P}_{II}$ represent the contribution of the metric variations δS to $\delta\mathcal{M}$ and $\delta\mathcal{P}$.

In the steady state, the constraint equation (13) specifies the variation of the state vector δw by

$$\frac{\partial}{\partial\xi_i}\delta\left(F_i - F_{vi}\right) = 0. \tag{17}$$

Here δF_i and δF_{vi} can also be split into contributions associated with δw and δS using the notation

$$\begin{aligned} \delta F_i &= \left[F_{iw}\right]_I \delta w + \delta F_{i\,II} \\ \delta F_{vi} &= \left[F_{viw}\right]_I \delta w + \delta F_{vi\,II}. \end{aligned} \tag{18}$$

The inviscid contributions are easily evaluated as

$$\left[F_{iw}\right]_I = S_{ij}\frac{\partial f_j}{\partial w}, \quad \delta F_{vi\,II} = \delta S_{ij} f_j.$$

The details of the viscous contributions are complicated by the additional level of derivatives in the stress and heat flux terms and will be derived in Section 6. Multiplying by a co-state vector ψ, which will play an analogous role to the Lagrange multiplier introduced in equation (4), and integrating over the domain produces

$$\int_{\mathcal{D}} \psi^T \frac{\partial}{\partial\xi_i}\delta\left(F_i - F_{vi}\right) = 0. \tag{19}$$

If ψ is differentiable this may be integrated by parts to give

$$\int_{\mathcal{B}} n_i\psi^T\delta\left(F_i - F_{vi}\right) d\mathcal{B}_\xi - \int_{\mathcal{D}} \frac{\partial\psi^T}{\partial\xi_i}\delta\left(F_i - F_{vi}\right) d\mathcal{D}_\xi = 0. \tag{20}$$

Since the left hand expression equals zero, it may be subtracted from the variation in the cost function (15) to give

$$\begin{aligned} \delta I &= \int_{\mathcal{B}} \left[\delta\mathcal{M} - n_i\psi^T\delta\left(F_i - F_{vi}\right)\right] d\mathcal{B}_\xi \\ &+ \int_{\mathcal{D}} \left[\delta\mathcal{P} + \frac{\partial\psi^T}{\partial\xi_i}\delta\left(F_i - F_{vi}\right)\right] d\mathcal{D}_\xi. \end{aligned} \tag{21}$$

Now, since ψ is an arbitrary differentiable function, it may be chosen in such a way that δI no longer depends explicitly on the variation of the state vector δw. The gradient of the cost function can then be evaluated directly from the metric variations without having to recompute the variation δw resulting from the perturbation of each design variable.

Comparing equations (16) and (18), the variation δw may be eliminated from (21) by equating all field terms with subscript "I" to produce a differential adjoint system governing ψ

$$\frac{\partial \psi^T}{\partial \xi_i} \left[F_{iw} - F_{viw} \right]_I \; + \; \mathcal{P}_w = 0 \quad \text{in } \mathcal{D}. \tag{22}$$

The corresponding adjoint boundary condition is produced by equating the subscript "I" boundary terms in equation (21) to produce

$$n_i \psi^T \left[F_{iw} - F_{viw} \right]_I = \mathcal{M}_w \quad \text{on } \mathcal{B}. \tag{23}$$

The remaining terms from equation (21) then yield a simplified expression for the variation of the cost function which defines the gradient

$$\begin{aligned} \delta I &= \int_{\mathcal{B}} \left\{ \delta \mathcal{M}_{II} - n_i \psi^T \left[\delta F_i - \delta F_{vi} \right]_{II} \right\} d\mathcal{B}_\xi \\ &+ \int_{\mathcal{D}} \left\{ \delta \mathcal{P}_{II} + \frac{\partial \psi^T}{\partial \xi_i} \left[\delta F_i - \delta F_{vi} \right]_{II} \right\} d\mathcal{D}_\xi. \end{aligned} \tag{24}$$

The details of the formula for the gradient depend on the way in which the boundary shape is parameterized as a function of the design variables, and the way in which the mesh is deformed as the boundary is modified. Using the relationship between the mesh deformation and the surface modification, the field integral is reduced to a surface integral by integrating along the coordinate lines emanating from the surface. Thus the expression for δI is finally reduced to the form of equation (6)

$$\delta I = \int_{\mathcal{B}} \mathcal{G} \delta \mathcal{F} \, d\mathcal{B}_\xi$$

where $\mathcal{F}$ represents the design variables, and $\mathcal{G}$ is the gradient, which is a function defined over the boundary surface.

The boundary conditions satisfied by the flow equations restrict the form of the left hand side of the adjoint boundary condition (23). Consequently, the boundary contribution to the cost function $\mathcal{M}$ cannot be specified arbitrarily. Instead, it must be chosen from the class of functions which allow cancellation of all terms containing δw in the boundary integral of equation (21). On the other hand, there is no such restriction on the specification of the field contribution to the cost function $\mathcal{P}$, since these terms may always be absorbed into the adjoint field equation (22) as source terms.

It is convenient to develop the inviscid and viscous contributions to the adjoint equations separately. Also, for simplicity, it will be assumed that the portion of the boundary that undergoes shape modifications is restricted to the coordinate surface $\xi_2 = 0$. Then equations (21) and (23) may be simplified by incorporating the conditions

$$n_1 = n_3 = 0, \quad n_2 = 1, \quad d\mathcal{B}_\xi = d\xi_1 d\xi_3,$$

so that only the variations δF_2 and δF_{v2} need to be considered at the wall boundary.

5 DERIVATION OF THE INVISCID ADJOINT TERMS

The inviscid contributions have been previously derived in[5,18] but are included here for completeness. Taking the transpose of equation (22), the inviscid adjoint equation may be written as

$$C_i^T \frac{\partial \psi}{\partial \xi_i} = 0 \quad \text{in } \mathcal{D}, \tag{25}$$

where the inviscid Jacobian matrices in the transformed space are given by

$$C_i = S_{ij} \frac{\partial f_j}{\partial w}.$$

The transformed velocity components have the form

$$U_i = S_{ij} u_j,$$

and the condition that there is no flow through the wall boundary at $\xi_2 = 0$ is equivalent to

$$U_2 = 0,$$

so that

$$\delta U_2 = 0$$

when the boundary shape is modified. Consequently the variation of the inviscid flux at the boundary reduces to

$$\delta F_2 = \delta p \begin{Bmatrix} 0 \\ S_{21} \\ S_{22} \\ S_{23} \\ 0 \end{Bmatrix} + p \begin{Bmatrix} 0 \\ \delta S_{21} \\ \delta S_{22} \\ \delta S_{23} \\ 0 \end{Bmatrix}. \tag{26}$$

Since δF_2 depends only on the pressure, it is now clear that the performance measure on the boundary $\mathcal{M}(w, S)$ may only be a function of the pressure and metric terms. Otherwise, complete cancellation of the terms containing δw in the boundary integral would be impossible. One may, for example, include arbitrary measures of the forces and moments in the cost function, since these are functions of the surface pressure.

In order to design a shape which will lead to a desired pressure distribution, a natural choice is to set

$$I = \frac{1}{2} \int_{\mathcal{B}} (p - p_d)^2 \, dS$$

where p_d is the desired surface pressure, and the integral is evaluated over the actual surface area. In the computational domain this is transformed to

$$I = \frac{1}{2} \int\int_{\mathcal{B}_w} (p - p_d)^2 \, |S_2| \, d\xi_1 d\xi_3,$$

where the quantity

$$|S_2| = \sqrt{S_{2j} S_{2j}}$$

denotes the face area corresponding to a unit element of face area in the computational domain. Now, to cancel the dependence of the boundary integral on δp, the adjoint boundary condition reduces to

$$\psi_j n_j = p - p_d \tag{27}$$

where n_j are the components of the surface normal

$$n_j = \frac{S_{2j}}{|S_2|}.$$

This amounts to a transpiration boundary condition on the co-state variables corresponding to the momentum components. Note that it imposes no restriction on the tangential component of ψ at the boundary.

In the presence of shock waves, neither p nor p_d are necessarily continuous at the surface. The boundary condition is then in conflict with the assumption that ψ is differentiable. This difficulty can be circumvented by the use of a smoothed boundary condition [18].

6 DERIVATION OF THE VISCOUS ADJOINT TERMS

In computational coordinates, the viscous terms in the Navier–Stokes equations have the form

$$\frac{\partial F_{vi}}{\partial \xi_i} = \frac{\partial}{\partial \xi_i}\left(S_{ij} f_{vj}\right).$$

Computing the variation δw resulting from a shape modification of the boundary, introducing a co-state vector ψ and integrating by parts following the steps outlined by equations (17) to (20) produces

$$\begin{aligned} & \int_{\mathcal{B}} \psi^T \left(\delta S_{2j} f_{vj} + S_{2j} \delta f_{vj}\right) d\mathcal{B}_\xi \\ - & \int_{\mathcal{D}} \frac{\partial \psi^T}{\partial \xi_i} \left(\delta S_{ij} f_{vj} + S_{ij} \delta f_{vj}\right) d\mathcal{D}_\xi, \end{aligned}$$

where the shape modification is restricted to the coordinate surface $\xi_2 = 0$ so that $n_1 = n_3 = 0$, and $n_2 = 1$. Furthermore, it is assumed that the boundary contributions at the far field may either be neglected or else eliminated by a proper choice of boundary conditions as previously shown for the inviscid case [5,18].

The viscous terms will be derived under the assumption that the viscosity and heat conduction coefficients μ and k are essentially independent of the flow, and that their variations may be neglected. In the case of turbulent flow, if the flow variations are found to result in significant changes in the turbulent viscosity, it may eventually be necessary to include its variation in the calculations.

Transformation to Primitive Variables

The derivation of the viscous adjoint terms is simplified by transforming to the primitive variables

$$\tilde{w}^T = (\rho, u_1, u_2, u_3, p)^T,$$

because the viscous stresses depend on the velocity derivatives $\frac{\partial u_i}{\partial x_j}$, while the heat flux can be expressed as

$$\kappa \frac{\partial}{\partial x_i}\left(\frac{p}{\rho}\right).$$

where $\kappa = \frac{k}{R} = \frac{\gamma\mu}{Pr(\gamma-1)}$. The relationship between the conservative and primitive variations is defined by the expressions

$$\delta w = M \delta \tilde{w}, \quad \delta \tilde{w} = M^{-1} \delta w$$

which make use of the transformation matrices $M = \frac{\partial w}{\partial \tilde{w}}$ and $M^{-1} = \frac{\partial \tilde{w}}{\partial w}$. These matrices are provided in transposed form for future convenience

$$M^T = \begin{bmatrix} 1 & u_1 & u_2 & u_3 & \frac{u_i u_i}{2} \\ 0 & \rho & 0 & 0 & \rho u_1 \\ 0 & 0 & \rho & 0 & \rho u_2 \\ 0 & 0 & 0 & \rho & \rho u_3 \\ 0 & 0 & 0 & 0 & \frac{1}{\gamma-1} \end{bmatrix}$$

$$M^{-1^T} = \begin{bmatrix} 1 & -\frac{u_1}{\rho} & -\frac{u_2}{\rho} & -\frac{u_3}{\rho} & \frac{(\gamma-1)u_i u_i}{2} \\ 0 & \frac{1}{\rho} & 0 & 0 & -(\gamma-1)u_1 \\ 0 & 0 & \frac{1}{\rho} & 0 & -(\gamma-1)u_2 \\ 0 & 0 & 0 & \frac{1}{\rho} & -(\gamma-1)u_3 \\ 0 & 0 & 0 & 0 & \gamma-1 \end{bmatrix}.$$

The conservative and primitive adjoint operators L and $\tilde{L}$ corresponding to the variations δw and $\delta \tilde{w}$ are then related by

$$\int_{\mathcal{D}} \delta w^T L \psi \, d\mathcal{D}_\xi = \int_{\mathcal{D}} \delta \tilde{w}^T \tilde{L} \psi \, d\mathcal{D}_\xi,$$

with

$$\tilde{L} = M^T L,$$

so that after determining the primitive adjoint operator by direct evaluation of the viscous portion of (22), the conservative operator may be obtained by the transformation $L = {M^{-1}}^T \tilde{L}$. Since the continuity equation contains no viscous terms, it makes no contribution to the viscous adjoint system. Therefore, the derivation proceeds by first examining the adjoint operators arising from the momentum equations.

Contributions from the Momentum Equations

In order to make use of the summation convention, it is convenient to set $\psi_{j+1} = \phi_j$ for $j = 1, 2, 3$. Then the contribution from the momentum equations is

$$\begin{aligned} &\int_{\mathcal{B}} \phi_k \left(\delta S_{2j}\sigma_{kj} + S_{2j}\delta\sigma_{kj}\right) d\mathcal{B}_\xi \\ -&\int_{\mathcal{D}} \frac{\partial \phi_k}{\partial \xi_i} \left(\delta S_{ij}\sigma_{kj} + S_{ij}\delta\sigma_{kj}\right) d\mathcal{D}_\xi. \end{aligned} \tag{28}$$

The velocity derivatives in the viscous stresses can be expressed as

$$\frac{\partial u_i}{\partial x_j} = \frac{\partial u_i}{\partial \xi_l}\frac{\partial \xi_l}{\partial x_j} = \frac{S_{lj}}{J}\frac{\partial u_i}{\partial \xi_l}$$

with corresponding variations

$$\delta\frac{\partial u_i}{\partial x_j} = \left[\frac{S_{lj}}{J}\right]_I \frac{\partial}{\partial \xi_l}\delta u_i + \left[\frac{\partial u_i}{\partial \xi_l}\right]_{II} \delta\left(\frac{S_{lj}}{J}\right).$$

The variations in the stresses are then

$$\begin{aligned} \delta\sigma_{kj} \;=\; & \left\{\mu\left[\tfrac{S_{lj}}{J}\tfrac{\partial}{\partial\xi_l}\delta u_k + \tfrac{S_{lk}}{J}\tfrac{\partial}{\partial\xi_l}\delta u_j\right]\right. \\ & \qquad \left. + \lambda\left[\delta_{jk}\tfrac{S_{lm}}{J}\tfrac{\partial}{\partial\xi_l}\delta u_m\right]\right\}_I \\ + \; & \left\{\mu\left[\delta\left(\tfrac{S_{lj}}{J}\right)\tfrac{\partial u_k}{\partial\xi_l} + \delta\left(\tfrac{S_{lk}}{J}\right)\tfrac{\partial u_j}{\partial\xi_l}\right]\right. \\ & \qquad \left. + \lambda\left[\delta_{jk}\delta\left(\tfrac{S_{lm}}{J}\right)\tfrac{\partial u_m}{\partial\xi_l}\right]\right\}_{II}. \end{aligned}$$

As before, only those terms with subscript I, which contain variations of the flow variables, need be considered further in deriving the adjoint operator. The field contributions that contain δu_i in equation (28) appear as

$$\begin{aligned} -\int_{\mathcal{D}} \frac{\partial \phi_k}{\partial \xi_i} S_{ij} \left\{\mu\left(\frac{S_{lj}}{J}\frac{\partial}{\partial\xi_l}\delta u_k + \frac{S_{lk}}{J}\frac{\partial}{\partial\xi_l}\delta u_j\right)\right. \\ \left. + \lambda\delta_{jk}\frac{S_{lm}}{J}\frac{\partial}{\partial\xi_l}\delta u_m\right\} d\mathcal{D}_\xi. \end{aligned}$$

This may be integrated by parts to yield

$$\begin{aligned} &\int_{\mathcal{D}} \delta u_k \frac{\partial}{\partial\xi_l}\left(S_{lj}S_{ij}\frac{\mu}{J}\frac{\partial\phi_k}{\partial\xi_i}\right) d\mathcal{D}_\xi \\ + \;& \int_{\mathcal{D}} \delta u_j \frac{\partial}{\partial\xi_l}\left(S_{lk}S_{ij}\frac{\mu}{J}\frac{\partial\phi_k}{\partial\xi_i}\right) d\mathcal{D}_\xi \\ + \;& \int_{\mathcal{D}} \delta u_m \frac{\partial}{\partial\xi_l}\left(S_{lm}S_{ij}\frac{\lambda\delta_{jk}}{J}\frac{\partial\phi_k}{\partial\xi_i}\right) d\mathcal{D}_\xi, \end{aligned}$$

where the boundary integral has been eliminated by noting that $\delta u_i = 0$ on the solid boundary. By exchanging indices, the field integrals may be combined to produce

$$\int_{\mathcal{D}} \delta u_k \frac{\partial}{\partial \xi_l} S_{lj} \left\{ \mu \left(\frac{S_{ij}}{J} \frac{\partial \phi_k}{\partial \xi_i} + \frac{S_{ik}}{J} \frac{\partial \phi_j}{\partial \xi_i} \right) + \lambda \delta_{jk} \frac{S_{im}}{J} \frac{\partial \phi_m}{\partial \xi_i} \right\} d\mathcal{D}_\xi,$$

which is further simplified by transforming the inner derivatives back to Cartesian coordinates

$$\int_{\mathcal{D}} \delta u_k \frac{\partial}{\partial \xi_l} S_{lj} \left\{ \mu \left(\frac{\partial \phi_k}{\partial x_j} + \frac{\partial \phi_j}{\partial x_k} \right) + \lambda \delta_{jk} \frac{\partial \phi_m}{\partial x_m} \right\} d\mathcal{D}_\xi. \tag{29}$$

The boundary contributions that contain δu_i in equation (28) may be simplified using the fact that

$$\frac{\partial}{\partial \xi_l} \delta u_i = 0 \quad \text{if} \quad l = 1, 3$$

on the boundary $\mathcal{B}$ so that they become

$$\int_{\mathcal{B}} \phi_k S_{2j} \left\{ \mu \left(\frac{S_{2j}}{J} \frac{\partial}{\partial \xi_2} \delta u_k + \frac{S_{2k}}{J} \frac{\partial}{\partial \xi_2} \delta u_j \right) + \lambda \delta_{jk} \frac{S_{2m}}{J} \frac{\partial}{\partial \xi_2} \delta u_m \right\} dS_x. \tag{30}$$

Together, (29) and (30) comprise the field and boundary contributions of the momentum equations to the viscous adjoint operator in primitive variables.

Contributions from the Energy Equation

In order to derive the contribution of the energy equation to the viscous adjoint terms it is convenient to set

$$\psi_5 = \theta, \quad Q_j = u_i \sigma_{ij} + \kappa \frac{\partial}{\partial x_j} \left(\frac{p}{\rho} \right),$$

where the temperature has been written in terms of pressure and density using (12). The contribution from the energy equation can then be written as

$$\int_{\mathcal{B}} \theta \left(\delta S_{2j} Q_j + S_{2j} \delta Q_j \right) d\mathcal{B}_\xi - \int_{\mathcal{D}} \frac{\partial \theta}{\partial \xi_i} \left(\delta S_{ij} Q_j + S_{ij} \delta Q_j \right) d\mathcal{D}_\xi. \tag{31}$$

The field contributions that contain δu_i,δp, and $\delta \rho$ in equation (31) appear as

$$-\int_{\mathcal{D}} \frac{\partial \theta}{\partial \xi_i} S_{ij} \delta Q_j d\mathcal{D}_\xi = -\int_{\mathcal{D}} \frac{\partial \theta}{\partial \xi_i} S_{ij} \left\{ \delta u_k \sigma_{kj} + u_k \delta \sigma_{kj} + \kappa \frac{S_{lj}}{J} \frac{\partial}{\partial \xi_l} \left(\frac{\delta p}{\rho} - \frac{p}{\rho} \frac{\delta \rho}{\rho} \right) \right\} d\mathcal{D}_\xi. \tag{32}$$

The term involving $\delta \sigma_{kj}$ may be integrated by parts to produce

$$\int_{\mathcal{D}} \delta u_k \frac{\partial}{\partial \xi_l} S_{lj} \left\{ \mu \left(u_k \frac{\partial \theta}{\partial x_j} + u_j \frac{\partial \theta}{\partial x_k} \right) + \lambda \delta_{jk} u_m \frac{\partial \theta}{\partial x_m} \right\} d\mathcal{D}_\xi, \tag{33}$$

where the conditions $u_i = \delta u_i = 0$ are used to eliminate the boundary integral on $\mathcal{B}$. Notice that the other term in (32) that involves δu_k need not be integrated by parts and is merely carried on as

$$-\int_{\mathcal{D}} \delta u_k \sigma_{kj} S_{ij} \frac{\partial \theta}{\partial \xi_i} d\mathcal{D}_\xi \tag{34}$$

The terms in expression (32) that involve δp and $\delta \rho$ may also be integrated by parts to produce both a field and a boundary integral. The field integral becomes

$$\int_{\mathcal{D}} \left(\frac{\delta p}{\rho} - \frac{p}{\rho} \frac{\delta \rho}{\rho} \right) \frac{\partial}{\partial \xi_l} \left(S_{lj} S_{ij} \frac{\kappa}{J} \frac{\partial \theta}{\partial \xi_i} \right) d\mathcal{D}_\xi$$

which may be simplified by transforming the inner derivative to Cartesian coordinates

$$\int_{\mathcal{D}} \left(\frac{\delta p}{\rho} - \frac{p}{\rho} \frac{\delta \rho}{\rho} \right) \frac{\partial}{\partial \xi_l} \left(S_{lj} \kappa \frac{\partial \theta}{\partial x_j} \right) d\mathcal{D}_\xi. \tag{35}$$

The boundary integral becomes

$$\int_{\mathcal{B}} \kappa \left(\frac{\delta p}{\rho} - \frac{p}{\rho} \frac{\delta \rho}{\rho} \right) \frac{S_{2j} S_{ij}}{J} \frac{\partial \theta}{\partial \xi_i} d\mathcal{B}_\xi. \tag{36}$$

This can be simplified by transforming the inner derivative to Cartesian coordinates

$$\int_{\mathcal{B}} \kappa \left(\frac{\delta p}{\rho} - \frac{p}{\rho} \frac{\delta \rho}{\rho} \right) \frac{S_{2j}}{J} \frac{\partial \theta}{\partial x_j} d\mathcal{B}_\xi, \tag{37}$$

and identifying the normal derivative at the wall

$$\frac{\partial}{\partial n} = S_{2j} \frac{\partial}{\partial x_j}, \tag{38}$$

and the variation in temperature

$$\delta T = \frac{1}{R} \left(\frac{\delta p}{\rho} - \frac{p}{\rho} \frac{\delta \rho}{\rho} \right),$$

to produce the boundary contribution

$$\int_{\mathcal{B}} k \delta T \frac{\partial \theta}{\partial n} d\mathcal{B}_\xi. \tag{39}$$

This term vanishes if T is constant on the wall but persists if the wall is adiabatic.

There is also a boundary contribution left over from the first integration by parts (31) which has the form

$$\int_{\mathcal{B}} \theta \delta \left(S_{2j} Q_j \right) d\mathcal{B}_\xi, \tag{40}$$

where

$$Q_j = k \frac{\partial T}{\partial x_j},$$

since $u_i = 0$. Notice that for future convenience in discussing the adjoint boundary conditions resulting from the energy equation, both the δw and δS terms corresponding to subscript classes I and II are considered simultaneously. If the wall is adiabatic

$$\frac{\partial T}{\partial n} = 0,$$

so that using (38),

$$\delta \left(S_{2j} Q_j \right) = 0,$$

and both the δw and δS boundary contributions vanish.

On the other hand, if T is constant $\frac{\partial T}{\partial \xi_l} = 0$ for $l = 1, 3$, so that

$$Q_j = k\frac{\partial T}{\partial x_j} = k\left(\frac{S_{lj}}{J}\frac{\partial T}{\partial \xi_l}\right) = k\left(\frac{S_{2j}}{J}\frac{\partial T}{\partial \xi_2}\right).$$

Thus, the boundary integral (40) becomes

$$\int_{\mathcal{B}} k\theta\left\{\frac{{S_{2j}}^2}{J}\frac{\partial}{\partial \xi_2}\delta T + \delta\left(\frac{{S_{2j}}^2}{J}\right)\frac{\partial T}{\partial \xi_2}\right\} d\mathcal{B}_\xi \ . \tag{41}$$

Therefore, for constant T, the first term corresponding to variations in the flow field contributes to the adjoint boundary operator and the second set of terms corresponding to metric variations contribute to the cost function gradient.

All together, the contributions from the energy equation to the viscous adjoint operator are the three field terms (33), (34) and (35), and either of two boundary contributions (39) or (41), depending on whether the wall is adiabatic or has constant temperature.

7 THE VISCOUS ADJOINT FIELD OPERATOR

Collecting together the contributions from the momentum and energy equations, the viscous adjoint operator in primitive variables can be expressed as

$$\begin{aligned}
(\tilde{L}\psi)_1 &= -\frac{p}{\rho^2}\frac{\partial}{\partial \xi_l}\left(S_{lj}\kappa\frac{\partial \theta}{\partial x_j}\right) \\
(\tilde{L}\psi)_{i+1} &= \frac{\partial}{\partial \xi_l}\left\{S_{lj}\left[\mu\left(\frac{\partial \phi_i}{\partial x_j} + \frac{\partial \phi_j}{\partial x_i}\right) + \lambda\delta_{ij}\frac{\partial \phi_k}{\partial x_k}\right]\right\} \qquad i = 1, 2, 3 \\
&+ \frac{\partial}{\partial \xi_l}\left\{S_{lj}\left[\mu\left(u_i\frac{\partial \theta}{\partial x_j} + u_j\frac{\partial \theta}{\partial x_i}\right) + \lambda\delta_{ij}u_k\frac{\partial \theta}{\partial x_k}\right]\right\} \\
&- \sigma_{ij}S_{lj}\frac{\partial \theta}{\partial \xi_l} \\
(\tilde{L}\psi)_5 &= \rho\frac{\partial}{\partial \xi_l}\left(S_{lj}\kappa\frac{\partial \theta}{\partial x_j}\right).
\end{aligned}$$

The conservative viscous adjoint operator may now be obtained by the transformation

$$L = {M^{-1}}^T\tilde{L}.$$

8 VISCOUS ADJOINT BOUNDARY CONDITIONS

It was recognized in Section 4 that the boundary conditions satisfied by the flow equations restrict the form of the performance measure that may be chosen for the cost function. There must be a direct correspondence between the flow variables for which variations appear in the variation of the cost function, and those variables for which variations appear in the boundary terms arising during the derivation of the adjoint field equations. Otherwise it would be impossible to eliminate the dependence of δI on δw through proper specification of the adjoint boundary condition. As in the derivation of the field equations, it proves convenient to consider the contributions from the momentum equations and the energy equation separately.

Boundary Conditions Arising from the Momentum Equations

The boundary term that arises from the momentum equations including both the δw and δS components (28) takes the form

$$\int_{\mathcal{B}} \phi_k\delta\left(S_{2j}\sigma_{kj}\right) d\mathcal{B}_\xi.$$

Replacing the metric term with the corresponding local face area S_2 and unit normal n_j defined by

$$|S_2| = \sqrt{S_{2j}S_{2j}}, \quad n_j = \frac{S_{2j}}{|S_2|}$$

then leads to

$$\int_{\mathcal{B}} \phi_k \delta \left(|S_2| \, n_j \sigma_{kj} \right) d\mathcal{B}_\xi.$$

Defining the components of the surface stress as

$$\tau_k = n_j \sigma_{kj}$$

and the physical surface element

$$dS = |S_2| \, d\mathcal{B}_\xi,$$

the integral may then be split into two components

$$\int_{\mathcal{B}} \phi_k \tau_k \, |\delta S_2| \, d\mathcal{B}_\xi + \int_{\mathcal{B}} \phi_k \, |S_2| \, \delta\tau_k dS, \tag{42}$$

where only the second term contains variations in the flow variables and must consequently cancel the δw terms arising in the cost function. The first term will appear in the expression for the gradient.

A general expression for the cost function that allows cancellation with terms containing $\delta\tau_k$ has the form

$$I = \int_{\mathcal{B}} \mathcal{N}(\tau) dS, \tag{43}$$

corresponding to a variation

$$\delta I = \int_{\mathcal{B}} \frac{\partial \mathcal{N}}{\partial \tau_k} \delta\tau_k dS,$$

for which cancellation is achieved by the adjoint boundary condition

$$\phi_k = \frac{\partial \mathcal{N}}{\partial \tau_k}.$$

Natural choices for $\mathcal{N}$ arise from force optimization and as measures of the deviation of the surface stresses from desired target values.

For viscous force optimization, the cost function should measure friction drag. The friction force in the x_i direction is

$$CD_{fi} = \int_{\mathcal{B}} \sigma_{ij} dS_j = \int_{\mathcal{B}} S_{2j} \sigma_{ij} d\mathcal{B}_\xi$$

so that the force in a direction with cosines n_i has the form

$$C_{nf} = \int_{\mathcal{B}} n_i S_{2j} \sigma_{ij} d\mathcal{B}_\xi.$$

Expressed in terms of the surface stress τ_i, this corresponds to

$$C_{nf} = \int_{\mathcal{B}} n_i \tau_i dS,$$

so that basing the cost function (43) on this quantity gives

$$\mathcal{N} = n_i \tau_i.$$

Cancellation with the flow variation terms in equation (42) therefore mandates the adjoint boundary condition

$$\phi_k = n_k.$$

Note that this choice of boundary condition also eliminates the first term in equation (42) so that it need not be included in the gradient calculation.

In the inverse design case, where the cost function is intended to measure the deviation of the surface stresses from some desired target values, a suitable definition is

$$\mathcal{N}(\tau) = \frac{1}{2} a_{lk} \left(\tau_l - \tau_{dl}\right) \left(\tau_k - \tau_{dk}\right),$$

where τ_d is the desired surface stress, including the contribution of the pressure, and the coefficients a_{lk} define a weighting matrix. For cancellation

$$\phi_k \delta\tau_k = a_{lk} \left(\tau_l - \tau_{dl}\right) \delta\tau_k.$$

This is satisfied by the boundary condition

$$\phi_k = a_{lk} \left(\tau_l - \tau_{dl}\right). \tag{44}$$

Assuming arbitrary variations in $\delta\tau_k$, this condition is also necessary.

In order to control the surface pressure and normal stress one can measure the difference

$$n_j \left\{\sigma_{kj} + \delta_{kj} \left(p - p_d\right)\right\},$$

where p_d is the desired pressure. The normal component is then

$$\tau_n = n_k n_j \sigma_{kj} + p - p_d,$$

so that the measure becomes

$$\begin{aligned} \mathcal{N}(\tau) &= \frac{1}{2}\tau_n^2 \\ &= \frac{1}{2} n_l n_m n_k n_j \left\{\sigma_{lm} + \delta_{lm} \left(p - p_d\right)\right\} \\ &\cdot \quad \left\{\sigma_{kj} + \delta_{kj} \left(p - p_d\right)\right\}. \end{aligned}$$

This corresponds to setting

$$a_{lk} = n_l n_k$$

in equation (44). Defining the viscous normal stress as

$$\tau_{vn} = n_k n_j \sigma_{kj},$$

the measure can be expanded as

$$\begin{aligned} \mathcal{N}(\tau) &= \frac{1}{2} n_l n_m n_k n_j \sigma_{lm} \sigma_{kj} + \frac{1}{2} \left(n_k n_j \sigma_{kj} + n_l n_m \sigma_{lm}\right) \left(p - p_d\right) + \frac{1}{2} \left(p - p_d\right)^2 \\ &= \frac{1}{2}\tau_{vn}^2 + \tau_{vn} \left(p - p_d\right) + \frac{1}{2} \left(p - p_d\right)^2. \end{aligned}$$

For cancellation of the boundary terms

$$\phi_k \left(n_j \delta\sigma_{kj} + n_k \delta p\right) = \left\{n_l n_m \sigma_{lm} + n_l^2 \left(p - p_d\right)\right\} n_k \left(n_j \delta\sigma_{kj} + n_k \delta p\right)$$

leading to the boundary condition

$$\phi_k = n_k \left(\tau_{vn} + p - p_d\right).$$

In the case of high Reynolds number, this is well approximated by the equations

$$\phi_k = n_k \left(p - p_d\right), \tag{45}$$

which should be compared with the single scalar equation derived for the inviscid boundary condition (27). In the case of an inviscid flow, choosing

$$\mathcal{N}(\tau) = \frac{1}{2} \left(p - p_d\right)^2$$

requires

$$\phi_k n_k \delta p = \left(p - p_d\right) n_k^2 \delta p = \left(p - p_d\right) \delta p$$

which is satisfied by equation (45), but which represents an overspecification of the boundary condition since only the single condition (27) need be specified to ensure cancellation.

Boundary Conditions Arising from the Energy Equation

The form of the boundary terms arising from the energy equation depends on the choice of temperature boundary condition at the wall. For the adiabatic case, the boundary contribution is (39)

$$\int_{\mathcal{B}} k\delta T \frac{\partial \theta}{\partial n} d\mathcal{B}_\xi,$$

while for the constant temperature case the boundary term is (41). One possibility is to introduce a contribution into the cost function which is dependent T or $\frac{\partial T}{\partial n}$ so that the appropriate cancellation would occur. Since there is little physical intuition to guide the choice of such a cost function for aerodynamic design, a more natural solution is to set

$$\theta = 0$$

in the constant temperature case or

$$\frac{\partial \theta}{\partial n} = 0$$

in the adiabatic case. Note that in the constant temperature case, this choice of θ on the boundary would also eliminate the boundary metric variation terms in (40).

9 IMPLEMENTATION OF NAVIER-STOKES DESIGN

The design procedures can be summarized as follows:

1. Solve the flow equations for ρ, u_1, u_2,u_3, p.
2. Smooth the cost function, if necessary.
3. Solve the adjoint equations for ψ subject to appropriate boundary conditions.
4. Evaluate $\mathcal{G}$.
5. Project $\mathcal{G}$ into an allowable subspace that satisfies any geometric constraints.
6. Update the shape based on the direction of steepest descent.
7. Return to 1.

Practical implementation of the viscous design method relies heavily upon fast and accurate solvers for both the state (w) and co-state (ψ) systems. This work employs a well-validated Navier–Stokes solver developed by two of the authors [19].

Discretization

Both the flow and the adjoint equations are discretized using a semi-discrete cell-centered finite volume scheme. The convective fluxes across cell interfaces are represented by simple arithmetic averages of the fluxes computed using values from the cells on either side of the face, augmented by artificial diffusive terms to prevent numerical oscillations in the vicinity of shock waves. Continuing to use the summation convention for repeated indices, the numerical convective flux across the interface between cells A and B in a three dimensional mesh has the form

$$h_{AB} = \frac{1}{2} S_{AB_j} \left(f_{A_j} + f_{B_j} \right) - d_{AB},$$

where S_{AB_j} is the component of the face area in the j^{th} Cartesian coordinate direction, $\left(f_{A_j}\right)$ and $\left(f_{B_j}\right)$ denote the flux f_j as defined by equation (12) and d_{AB} is the diffusive term. Variations of the computer program provide options for alternate constructions of the diffusive flux.

The simplest option implements the Jameson-Schmidt-Turkel scheme [20,21], using scalar diffusive terms of the form

$$d_{AB} = \epsilon^{(2)} \Delta w - \epsilon^{(4)} \left(\Delta w^{+} - 2\Delta w + \Delta w^{-} \right),$$

where

$$\Delta w = w_B - w_A$$

and Δw^{+} and Δw^{-} are the same differences across the adjacent cell interfaces behind cell A and beyond cell B in the AB direction. By making the coefficient $\epsilon^{(2)}$ depend on a switch proportional to the undivided second difference of a flow quantity such as the pressure or entropy, the diffusive flux becomes a third order quantity, proportional to the cube of the mesh width in regions where the solution is smooth. Oscillations are suppressed near a shock wave because $\epsilon^{(2)}$ becomes of order unity, while $\epsilon^{(4)}$ is reduced to zero by the same switch. For a scalar conservation law, it is shown in reference [21] that $\epsilon^{(2)}$ and $\epsilon^{(4)}$ can be constructed to make the scheme satisfy the local extremum diminishing (LED) principle that local maxima cannot increase while local minima cannot decrease.

The second option applies the same construction to local characteristic variables. There are derived from the eigenvectors of the Jacobian matrix A_{AB} which exactly satisfies the relation

$$A_{AB} \left(w_B - w_A \right) = S_{AB_j} \left(f_{B_j} - f_{A_j} \right).$$

This corresponds to the definition of Roe [22]. The resulting scheme is LED in the characteristic variables. The third option implements the H-CUSP scheme proposed by Jameson [23] which combines differences $f_B - f_A$ and $w_B - w_A$ in a manner such that stationary shock waves can be captured with a single interior point in the discrete solution. This scheme minimizes the numerical diffusion as the velocity approaches zero in the boundary layer, and has therefore been preferred for viscous calculations in this work.

Similar artificial diffusive terms are introduced in the discretization of the adjoint equation, but with the opposite sign because the wave directions are reversed in the adjoint equation. Satisfactory results have been obtained using scalar diffusion in the adjoint equation while characteristic or H-CUSP constructions are used in the flow solution.

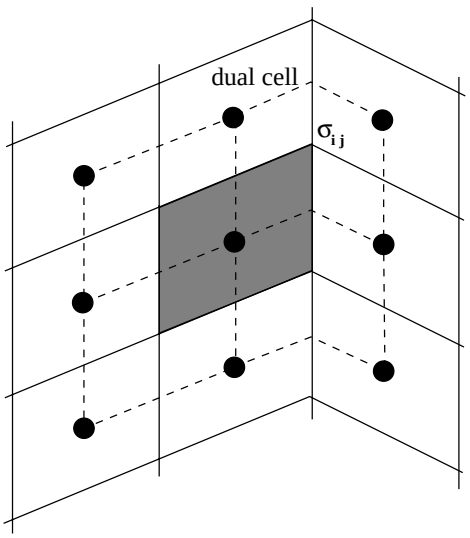

Figure 1: Cell-centered scheme. σ_{ij} evaluated at vertices of the primary mesh

The discretization of the viscous terms of the Navier Stokes equations requires the evaluation of the velocity derivatives $\frac{\partial_{u_i}}{\partial_{x_j}}$ in order to calculate the viscous stress tensor σ_{ij} defined in equation (11). These are most conveniently evaluated at the cell vertices of the primary mesh by introducing a

dual mesh which connects the cell centers of the primary mesh, as depicted in Figure (1). According to the Gauss formula for a control volume V with boundary S

$$\int_V \frac{\partial v_i}{\partial x_j} dv = \int_S u_i n_j dS$$

where n_j is the outward normal. Applied to the dual cells this yields the estimate

$$\frac{\partial v_i}{\partial x_j} = \frac{1}{\text{vol}} \sum_{\text{faces}} \bar{u}_i n_j S$$

where S is the area of a face, and $\bar{u}_i$ is an estimate of the average of u_i over that face. In order to determine the viscous flux balance of each primary cell, the viscous flux across each of its faces is then calculated from the average of the viscous stress tensor at the four vertices connected by that face. This leads to a compact scheme with a stencil connecting each cell to its 26 nearest neighbors.

The semi-discrete schemes for both the flow and the adjoint equations are both advanced to steady state by a multi-stage time stepping scheme. This is a generalized Runge-Kutta scheme in which the convective and diffusive terms are treated differently to enlarge the stability region [21,24]. Convergence to a steady state is accelerated by residual averaging and a multi-grid procedure [25]. Convergence is further accelerated by the use of locally varying time steps (which may be regarded as a scalar preconditioner) or the matrix preconditioner method developed by Pierce and Giles [16,17].

Optimization

For inverse design the lift is fixed by the target pressure. In drag minimization it is also appropriate to fix the lift coefficient, because the induced drag is a major fraction of the total drag, and this could be reduced simply by reducing the lift. Therefore the angle of attack is adjusted during the flow solution to force a specified lift coefficient to be attained.

The search procedure used in this work is a simple descent method in which small steps are taken in the negative gradient direction. Let $\mathcal{F}$ represent the design variable, and $\mathcal{G}$ the gradient. Then the iteration

$$\delta \mathcal{F} = -\lambda \mathcal{G}$$

can be regarded as simulating the time dependent process

$$\frac{d\mathcal{F}}{dt} = -\mathcal{G}$$

where λ is the time step Δt. Let A be the Hessian matrix with element

$$A_{ij} = \frac{\partial \mathcal{G}_i}{\partial \mathcal{F}_j} = \frac{\partial^2 I}{\partial \mathcal{F}_i \partial \mathcal{F}_j}.$$

Suppose that a locally minimum value of the cost function $I^* = I(\mathcal{F}^*)$ is attained when $\mathcal{F} = \mathcal{F}^*$. Then the gradient $\mathcal{G}^* = \mathcal{G}(\mathcal{F}^*)$ must be zero, while the Hessian matrix $A^* = A(\mathcal{F}^*)$ must be positive definite. Since $\mathcal{G}^*$ is zero, the cost function can be expanded as a Taylor series in the neighborhood of $\mathcal{F}^*$ with the form

$$I(\mathcal{F}) = I^* + \frac{1}{2} (\mathcal{F} - \mathcal{F}^*) A (\mathcal{F} - \mathcal{F}^*) + \dots$$

Correspondingly,

$$\mathcal{G}(\mathcal{F}) = A (\mathcal{F} - \mathcal{F}^*) + \dots$$

As $\mathcal{F}$ approaches $\mathcal{F}^*$, the leading terms become dominant. Then, setting $\hat{\mathcal{F}} = (\mathcal{F} - \mathcal{F}^*)$, the search process approximates

$$\frac{d\hat{\mathcal{F}}}{dt} = -A^* \hat{\mathcal{F}}.$$

Also, since A^* is positive definite it can be expanded as

$$A^* = RMR^T,$$

where M is a diagonal matrix containing the eigenvalues of A^*, and

$$RR^T = R^T R = I.$$

Setting

$$v = R^T \hat{\mathcal{F}},$$

the search process can be represented as

$$\frac{dv}{dt} = -Mv.$$

The stability region for the simple forward Euler stepping scheme is a unit circle centered at -1 on the negative real axis. Thus for stability we must choose

$$\mu_{\max} \Delta t = \mu_{\max} \lambda < 2,$$

while the asymptotic decay rate, given by the smallest eigenvalue, is proportional to

$$e^{-\mu_{\min} t}.$$

In order to improve the rate of convergence, one can set

$$\delta \mathcal{F} = -\lambda P \mathcal{G},$$

where P is a preconditioner for the search. An ideal choice is $P = A^{*-1}$, so that the corresponding time dependent process reduces to

$$\frac{d\hat{\mathcal{F}}}{dt} = -\hat{\mathcal{F}},$$

for which all the eigenvalues are equal to unity, and $\hat{\mathcal{F}}$ is reduced to zero in one time step by the choice $\Delta t = 1$. Quasi-Newton methods estimate A^* from the change in the gradient during the search process. This requires accurate estimates of the gradient at each time step. In order to obtain these, both the flow solution and the adjoint equation must be fully converged. Most quasi-Newton methods also require a line search in each search direction, for which the flow equations and cost function must be accurately evaluated several times. They have proven quite robust for aerodynamic optimization [7].

An alternative approach which has also proved successful in our previous work [18], and is used here, is to smooth the gradient and to replace $\mathcal{G}$ by its smoothed value $\bar{\mathcal{G}}$ in the descent process. This both acts as a preconditioner, and ensures that each new shape in the optimization sequence remains smooth. To apply smoothing in the ξ_1 direction, for example, the smoothed gradient $\bar{\mathcal{G}}$ ma be calculated from a discrete approximation to

$$\bar{\mathcal{G}} - \frac{\partial}{\partial \xi_1} \epsilon \frac{\partial}{\partial \xi_1} \bar{\mathcal{G}} = \mathcal{G}$$

where ϵ is the smoothing parameter. If one sets $\delta \mathcal{F} = -\lambda \bar{\mathcal{G}}$, then, assuming the modification is applied on the surface $\xi_2 =$ constant, the first order change in the cost function is

$$\begin{aligned}
\delta I &= -\int\int \mathcal{G} \delta \mathcal{F} \, d\xi_1 d\xi_3 \\
&= -\lambda \int\int \left(\bar{\mathcal{G}} - \frac{\partial}{\partial \xi_1} \epsilon \frac{\partial \bar{\mathcal{G}}}{\partial \xi_1} \right) \bar{\mathcal{G}} \, d\xi_1 d\xi_3 \\
&= -\lambda \int\int \left(\bar{\mathcal{G}}^2 + \epsilon \left(\frac{\partial \bar{\mathcal{G}}}{\partial \xi_1} \right)^2 \right) d\xi_1 d\xi_3 \\
&< 0,
\end{aligned}$$

assuring an improvement if λ is sufficiently small and positive, unless the process has already reached a stationary point at which $\mathcal{G} = 0$.

It turns out that this approach is tolerant to the use of approximate values of the gradient, so that neither the flow solution nor the adjoint solution need be fully converged before making a shape change. This results in very large savings in the computational cost. For inviscid optimization it is necessary to use only 15 multigrid cycles for the flow solution and the adjoint solution in each design iteration. For viscous optimization, about 100 multigrid cycles are needed. This is partly because convergence of the lift coefficient is much slower, so about 20 iterations must be made before each adjustment of the angle of attack to force the target lift coefficient. The new preconditioner for the flow and adjoint calculations allows the number of iterations to be substantially reduced in both the flow and the adjoint simulation.

The numerical tests so far have focused on the viscous design of wings for optimum cruise, for which the flow remains attached, and the main viscous effect is due to the displacement thickness of the boundary layer. While some tests have been made with the viscous adjoint terms included, it has been found that the optimization process converges when the viscous terms are omitted from the adjoint system. This may reflect the tolerance of the search process to inexact gradients.

10 RESULTS

Preconditioned Inverse Design

The first demonstration is an application of the preconditioning technique for inverse design with the Euler equations. The ONERA M6 (Figure 2b) wing is recovered for a lifting case starting from a wing with a NACA0012 section (Figure 2a) and using the ONERA M6 pressure distributions computed at $\alpha = 3.0$ and $M = 0.84$ as the target (Fig. 3). Thus, a symmetric wing section is to be recovered from an asymmetric pressure distribution. The calculations were performed on a 192×32×48 mesh with 294,912 cells. The mesh had a C-H topology with the C-lines wrapping around the wing leading edge. Each design cycle required 3 multigrid cycles for the flow solver using characteristic-based matrix dissipation with a matrix preconditioner and 12 multigrid cycles for the adjoint solver using scalar dissipation and a variable local time step (scalar preconditioner). Compared to a test in which the 3 multigrid cycles using the matrix preconditioner were replaced by 15 multigrid cycles using a standard scalar preconditioner, and 15 cycles were used in the adjoint solution, each design cycle required about 3/8 as much computer time, while the number of design cycles required to reach the same level of error also fell from 100 to about 50. Use of the matrix preconditioner therefore reduced the total CPU time on an IBM 590 workstation from 97,683 sec (∼27 hours) to 18,222 sec (∼5 hours) for roughly equivalent accuracy.

Viscous Design

Due to the high computational cost of viscous design, a two-stage design strategy is adopted. In the first stage, a design calculation is performed with the Euler equations to minimize the drag at a given lift coefficient by modifying the wing sections with a fixed planform. In the second stage, the pressure distribution of the Euler solution is used as the target pressure distribution for inverse design with the Navier-Stokes equations. Comparatively small modifications are required in the second stage, so that it can be accomplished with a small number of design cycles.

In order to test this strategy it was used for the re-design of a wing representative of wide-body transport aircraft. The results are shown in Figures 4 and 5. The design point was taken as a lift coefficient of .55 at a Mach number of .83. Figure 4 illustrates the Euler re-design, which was performed on a mesh with 192×32×48 cells, displaying both the geometry and the upper surface pressure distribution, with negative Cp upwards. The initial wing shows a moderately strong shock wave across most of the top surface, as can be seen in Figure 4a. Sixty design cycles were needed to produce the shock free wing shown in Figure 4b, with an indicated drag reduction of 15 counts from .0196 to .0181. Figure 5 shows the viscous re-design at a Reynolds number of 12 million. This was performed on a mesh with 192×64×48 cells, with 32 intervals normal to the wing concentrated inside the boundary layer region. In Figure 5a it can be seen that the Euler design produces a

weak shock due to the displacement effects of the boundary layer. Ten design cycles were needed to recover the shock free wing shown in Figure 5b. It is interesting that the wing section modifications between the initial wing of Figure 4a and the final wing of Figure 5b are remarkably small.

These results were sufficiently promising that it was decided by McDonnell Douglas to evaluate the method for industrial use, and it was used to support design studies for the MDXX project. The results of this experience are discussed in reference [26]. It rapidly became apparent that the fuselage effects are too large to be ignored. In viscous design it was also found that there were discrepancies between the results of the design calculations, which were initially performed on a relatively coarse grid with 192×64×48 cells, and the results of subsequent analysis calculations performed on finer meshes to verify the design.

In order to allow the use of finer meshes with overnight turnaround, the code was therefore modified for parallel computation. Using the parallel implementation, viscous design calculations have been performed on meshes with 1.8 million mesh points. Starting from a preliminary inviscid design, 20 design cycles are usually sufficient for a viscous re-design in inverse mode, with the smoothed inviscid results providing the target pressure. Such a calculation can be completed in about $7\frac{1}{2}$ hours using 48 processors of an IBM SP2.

As an illustration of the results that could be obtained, Figures 6 - 10 show a wing-body design with sweep back of about 38 degrees at the 1/4 chord. Starting from the result of an Euler design, the viscous optimization produced an essentially shock free wing at a cruise design point of Mach .86, with a lift coefficient of .6 for the wing body combination at a Reynolds number of 101 million based on the root chord. Figure 6 shows the design point, while the evolution of the design is shown in Figure 7, using Vassberg's COMPPLOT software. In this case the pressure contours are for the final design. This wing is quite thick, with a thickness to chord ratio of more than 14 percent at the root and 9 percent at the tip. The design offers excellent performance at the nominal cruise point. Figures 8 and 9 show the results of a Mach number sweep to determine the drag rise. It can be seen that a double shock pattern forms below the design point, while there is actually a slight increase in the drag coefficient of about 1 $\frac{1}{2}$ counts at Mach .85. Finally, Figure 10 shows a comparison of the pressure distribution at the design point with those at alternate cruise points with lower and higher lift. The tendency to produce double shocks below the design point is typical of supercritical wings. This wing has a low drag coefficient, however, over a wide range of conditions.

CONCLUSIONS

We have developed a three-dimensional control theory based design method for the Navier Stokes equations and applied it successfully to the design of wings in transonic flow. The method represents an extension of our previous work on design with the potential flow and Euler equations. The new method combines the versatility of numerical optimization methods with the efficiency of inverse design. The geometry is modified by a grid perturbation technique which is applicable to arbitrary configurations. The combination of computational efficiency with geometric flexibility provides a powerful tool, with the final goal being to create practical aerodynamic shape design methods for complete aircraft configurations. Such an accomplishment would represent the culmination of the line of research initiated by Lighthill with his original work on the inverse problem [1].

ACKNOWLEDGMENT

This work has benefited from the generous support of AFOSR under Grant No. AFOSR-91-0391, DOD/URI/ONR/ARPA N00014-92-J-1796, the NASA-IBM Cooperative Research Agreement, EPSRC and the Rhodes Trust.

1. M.J. Lighthill. A new method of two dimensional aerodynamic design. *R & M 1111*, Aeronautical Research Council, 1945.
2. J.L. Lions. *Optimal Control of Systems Governed by Partial Differential Equations.* Springer-Verlag, New York, 1971. Translated by S.K. Mitter.
3. A. Jameson. Aerodynamic design via control theory. *J. Sci. Comp.*, 3:233–260, 1988.

4. A. Jameson. Optimum aerodynamic design using CFD and control theory. AIAA Paper 95-1729-CP, 1995.
5. A. Jameson. Automatic design of transonic airfoils to reduce the shock induced pressure drag. In *Proceedings of the 31st Israel Annual Conference on Aviation and Aeronautics, Tel Aviv*, pages 5–17, February 1990.
6. J. Reuther and A. Jameson. Control based airfoil design using the Euler equations. *AIAA paper 94-4272-CP*, 1994.
7. J. Reuther and A. Jameson. Aerodynamic shape optimization of wing and wing-body configurations using control theory. *AIAA paper 95-0123*, AIAA 33rd Aerospace Sciences Meeting, Reno, Nevada, January 1995.
8. J. Reuther, A. Jameson, J. Farmer, L. Martinelli, and D. Saunders. Aerodynamic shape optimization of complex aircraft configurations via an adjoint method. *AIAA paper 96-0094*, AIAA 34th Aerospace Sciences Meeting, Reno, Nevada, January 1996.
9. O. Pironneau. *Optimal Shape Design for Elliptic Systems*. Springer-Verlag, New York, 1984.
10. O. Pironneau. Optimal shape design for aerodynamics. In *AGARD REPORT 803*, 1994.
11. S. Ta'asan, G. Kuruvila, and M. D. Salas. Aerodynamic design and optimization in one shot. *AIAA paper 92-005*, 30th Aerospace Sciences Meeting and Exibit, Reno, Nevada, January 1992.
12. O. Baysal and M. E. Eleshaky. Aerodynamic design optimization using sensitivity anaysis and computational fluid dynamics. *AIAA Journal*, 30(3):718–725, 1992.
13. H. Cabuk, C.H. Shung, and V. Modi. Adjoint operator approach to shape design for internal incompressible flow. In G.S. Dulikravich, editor, *Proceedings of the 3rd International Conference on Inverse Design and Optimization in Engineering Sciences*, pages 391–404, 1991.
14. J.C. Huan and V. Modi. Optimum design for drag minimizing bodies in incompressible flow. *Inverse Problems in Engineering*, 1:1–25, 1994.
15. M. Desai and K. Ito. Optimal controls of Navier-Stokes equations. *SIAM J. Control and Optimization*, 32(5):1428–1446, 1994.
16. N.A. Pierce and M.B. Giles. Preconditioning compressible flow calculations on stretched meshes. AIAA Paper 96-0889, 34th Aerospace Sciences Meeting and Exhibit, Reno, NV, 1996.
17. N.A. Pierce and M.B. Giles. Preconditioned multigrid methods for compressible flow calculations on stretched meshes. Submitted to *J. Comp. Phys.*, April, 1996.
18. A. Jameson. Optimum aerodynamic design using control theory. *Computational Fluid Dynamics Review*, pages 495–528, 1995.
19. L. Martinelli and A. Jameson. Validation of a multigrid method for the Reynolds averaged equations. *AIAA paper 88-0414*, 1988.
20. A. Jameson, W. Schmidt, and E. Turkel. Numerical solution of the Euler equations by finite volume methods using Runge-Kutta time stepping schemes. AIAA Paper 81-1259, 1981.
21. A. Jameson. Analysis and design of numerical schemes for gas dynamics 1, artificial diffusion, upwind biasing, limiters and their effect on multigrid convergence. *Int. J. of Comp. Fluid Dyn.*, 4:171–218, 1995.
22. P.L. Roe. Approximate Riemann solvers, parameter vectors, and difference schemes. *J. Comp. Phys.*, 43:357–372, 1981.
23. A. Jameson. Analysis and design of numerical schemes for gas dynamics 2, artificial diffusion and discrete shock structure. *Int. J. of Comp. Fluid Dyn.*, 5:1–38, 1995.
24. L. Martinelli. Calculations of viscous flows with a multigrid method. *Princeton University Thesis*, May 1987.
25. A. Jameson. Multigrid algorithms for compressible flow calculations. In W. Hackbusch and U. Trottenberg, editors, *Lecture Notes in Mathematics, Vol. 1228*, pages 166–201. Proceedings of the 2nd European Conference on Multigrid Methods, Cologne, 1985, Springer-Verlag, 1986.
26. A. Jameson. Re-Engineering the design process through camputation. *AIAA paper 97-0641*, January 1997.

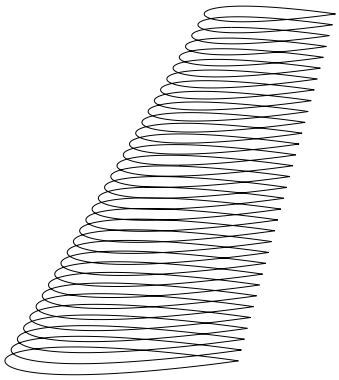

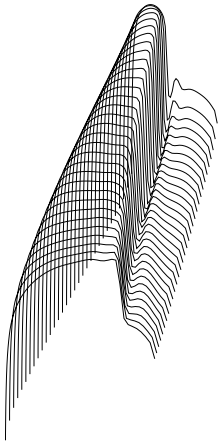

Initial Wing. C_p on Upper Surface.

Figure 2a: $M = .84, C_l = .3000, C_d = .0205, \alpha = 2.935°$.

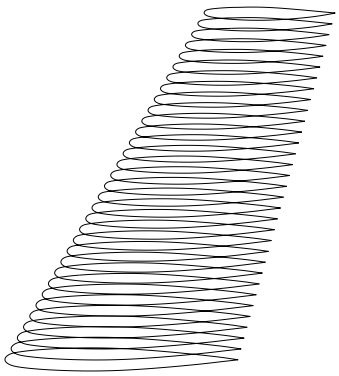

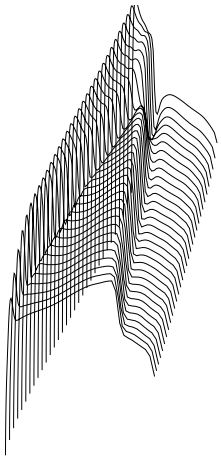

Re-designed wing. C_p on Upper Surface.

Figure 2b: $M = .84, C_l = .2967, C_d = .0141, \alpha = 2.935°$

Figure 2: Re-design of the Onera M6 Wing. 100 design cycles in inverse mode.

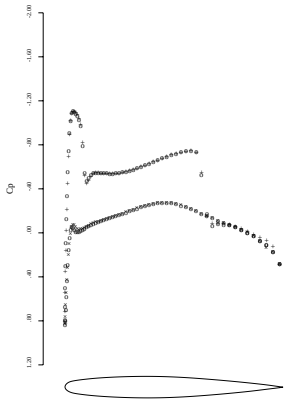

3a: span station $z = 0.297$

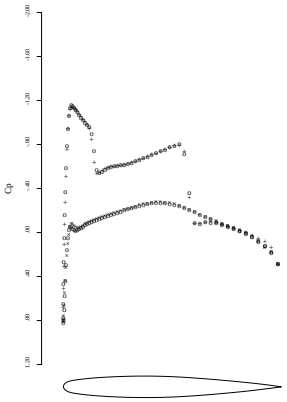

3b: span station $z = 0.484$

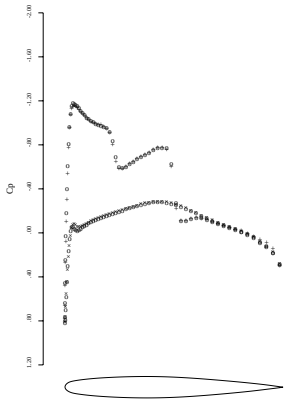

3c: span station $z = 0.672$

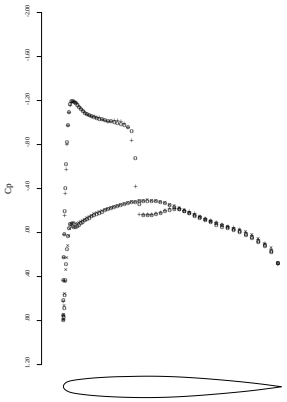

3d: span station $z = 0.859$

Figure 3: Target (o) and Computed ($+$) Pressure Distributions of Re-designed Onera M6 Wing. $M = 0.84$, $C_L = 0.2967$, $C_D = 0.0141$, $\alpha = 2.935^\circ$.

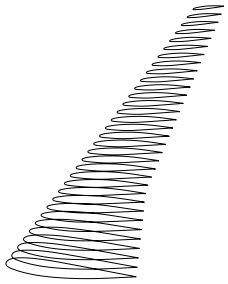

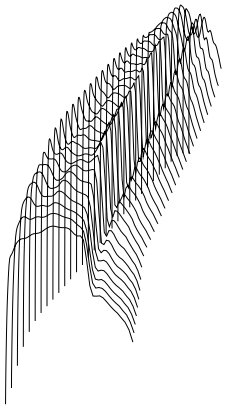

Initial Wing. C_p on Upper Surface.

Figure 4a: $M = .83, C_l = .5498, C_d = .0196, \alpha = 2.410°$.

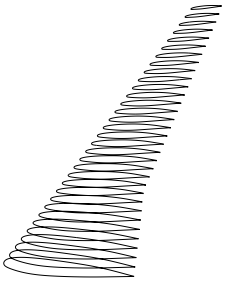

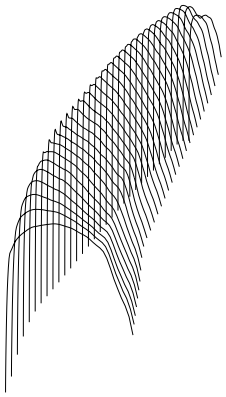

Redisigned wing. C_p on Upper Surface.

Figure 4b: $M = .83, C_l = .5500, C_d = .0181, \alpha = 1.959°$.

Figure 4: Re-design of the wing of a wide transport aircraft. Stage 1 Inviscid design : 60 design cycles in drag reduction mode with forced lift.

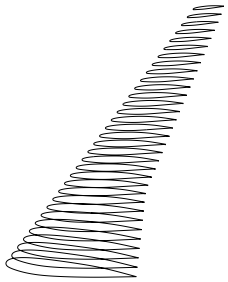

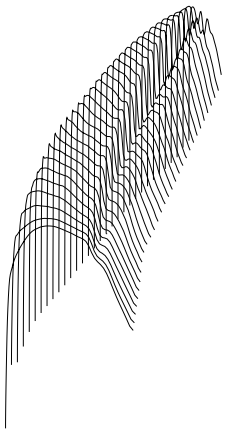

Initial Wing. C_p on Upper Surface.

Figure 5a: $M = 0.83, C_l = .5506, C_d = .0199, \alpha = 2.317^\circ$

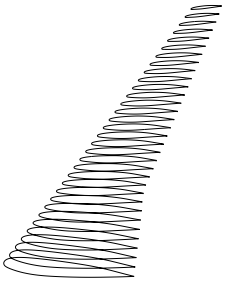

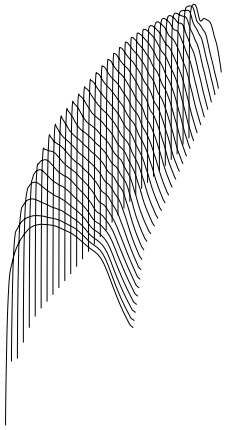

Redisigned wing. C_p on Upper Surface.

Figure 5b: $M = 0.83, C_l = .5508, C_d = .0194, \alpha = 2.355^\circ$

Figure 5: Re-design of the wing of a wide transport aircraft. Stage 2: Viscous re-design. 10 design cycles in inverse mode.

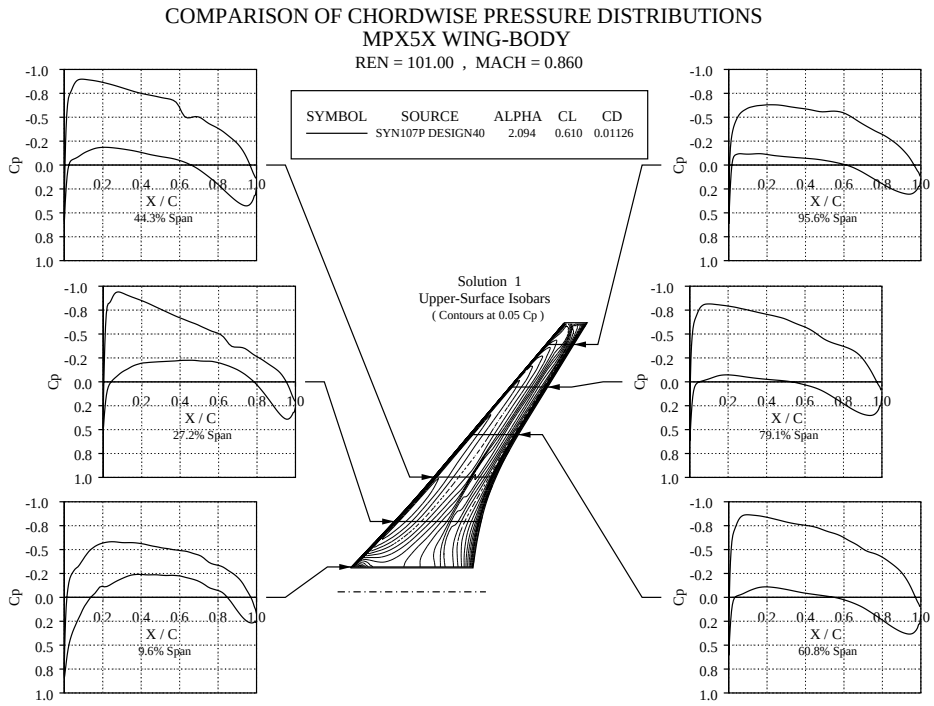

Figure 6: Pressure distribution of the MPX5X at its design point.

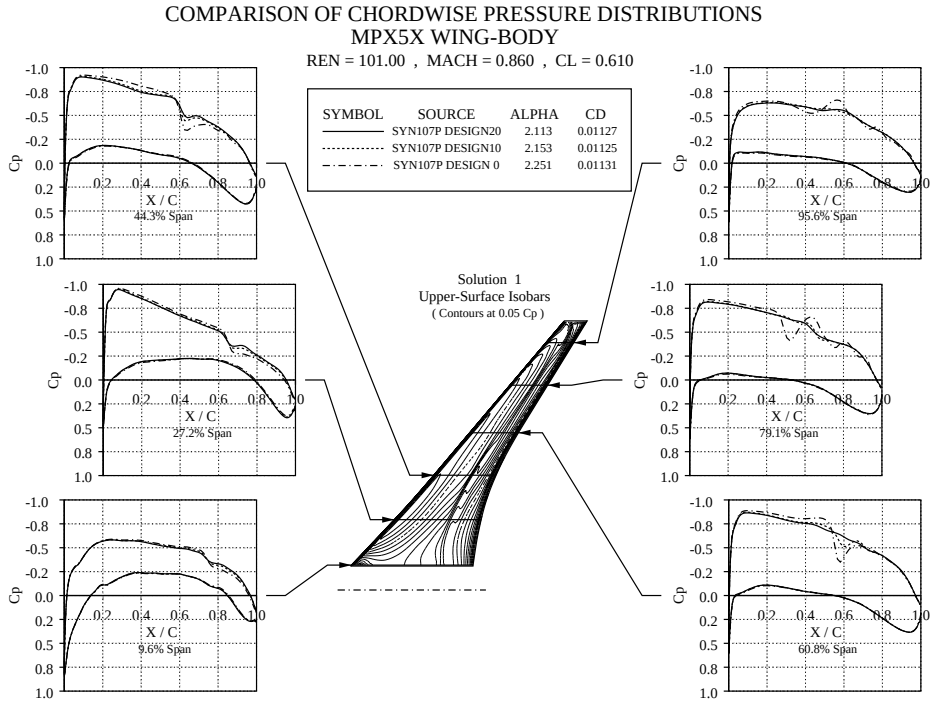

Figure 7: Optimization Sequence in the design of the MPX5X.

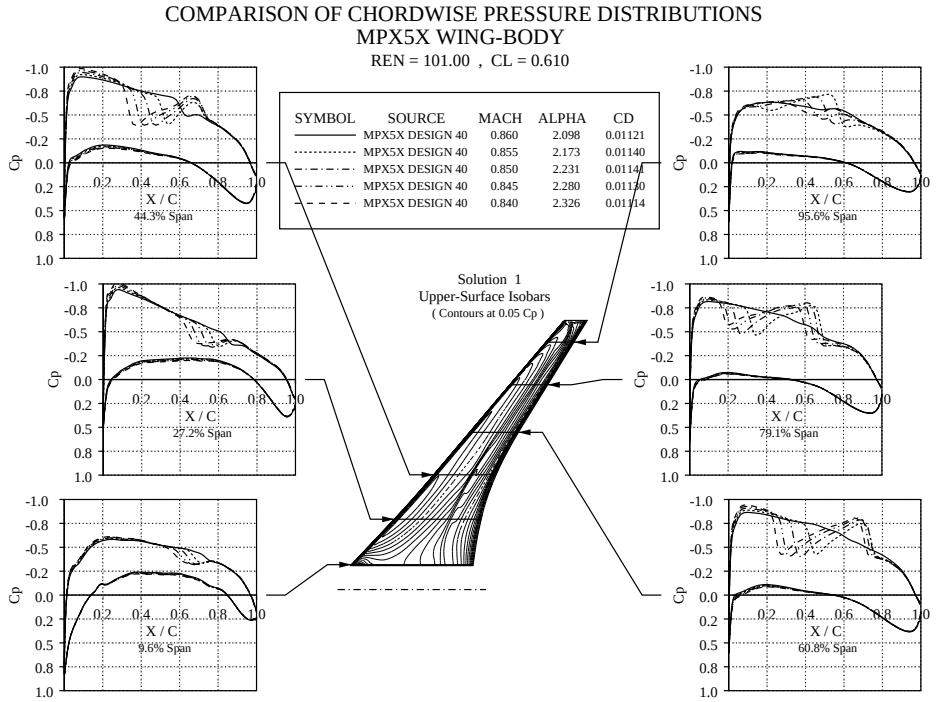

Figure 8: Off design performance of the MPX5X below the design point.

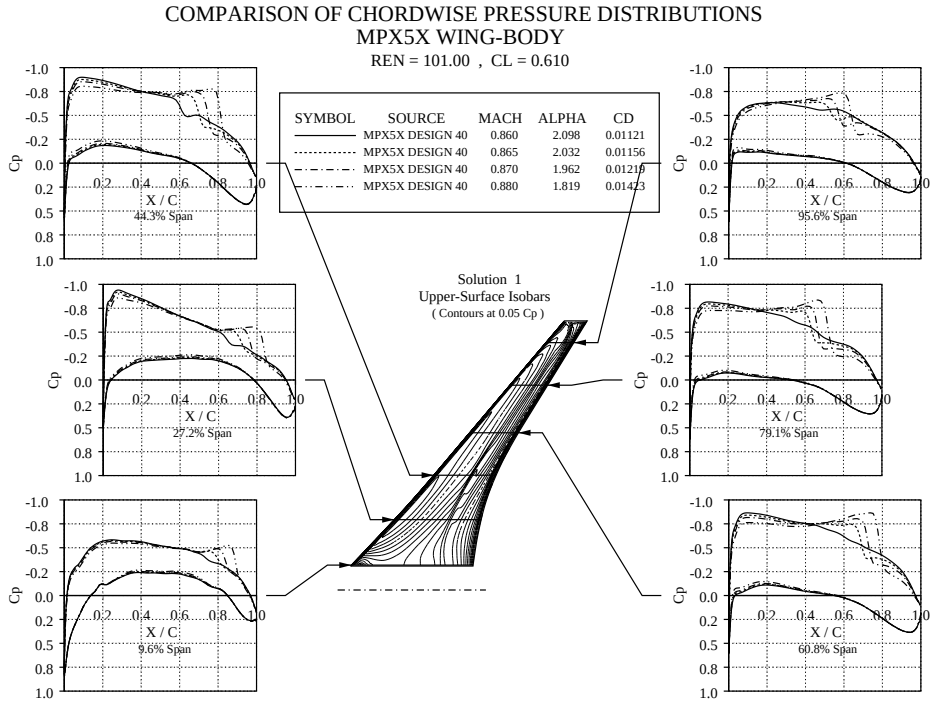

Figure 9: Off design performance of the MPX5X above the design point.

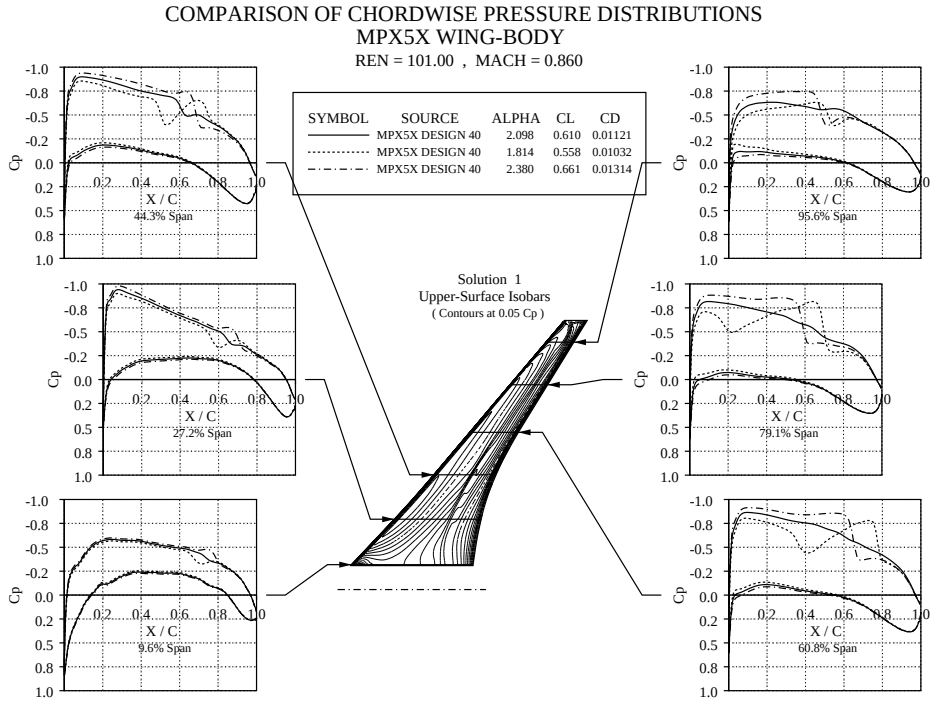

Figure 10: Comparison of the MPX5X at its design point and at lower and higher lift.